Int. J. Electrochem. Sci., 14 **(2019)** 9909 – 9920, doi: 10.20964/2019.10.51

International Journal of
ELECTROCHEMICAL
SCIENCE
www.electrochemsci.org

An Electrochemical Sensor for Dopamine Detection Based on Ternary Pd-Au-P Composites Supported on PDDA/RGO

Min Zhang[*], *Dongmei Fu*

School of Stomatology, Lanzhou University, Lanzhou 730000, China
[*]E-mail: zm@lzu.edu.cn

Received: 9 June 2019 / *Accepted:* 14 August 2019 / *Published:* 30 August 2019

A gas-liquid interface approach was developed for the synthesis of ternary Pd-Au-P composites, which were supported on poly(diallyldimethylammonium chloride)-functionalized reduced graphene oxide (PDDA/RGO). The as-synthesized composites were characterized by transmission electron microscopy (TEM), energy dispersive X-ray spectroscopy (EDX), X-ray diffraction (XRD) and X-ray photoelectron spectroscopy (XPS). The Pd-Au-P-PDDA/RGO composites as an electrochemical dopamine (DA) sensor showed superior electrocatalytic activity and stability toward DA oxidation as compared with Pd-Au-PDDA/RGO and Pd-Au-P/RGO. The enhanced electrochemical performance could be attributed to the effect of electronic structure and long-range disorder and short-range structure due to the doping of P element. By studying the kinetics of DA oxidation, electrochemical DA oxidation was proven to be irreversible and follow Laviron Equation. Using differential pulse voltammetry (DPV), the Pd-Au-P/PDDA/RGO sensor had low detection limit of 0.7 μM, wide linear range of 3.5-125 μM and relatively high sensitivity (0.2858 μA/μM), which was suitable for the detection of biological and environmental samples.

Keywords: Pd-Au-P; Reduced graphene oxide; Dopamine detection; Electrochemical sensor

1. INTRODUCTION

Nowadays, functional electronic materials are increasingly in demand for the development of electrochemical sensor. Compared with including fluorescence [1], chromatography [2] and colorimetric method [3], electrochemical techniques has the advantage of ease operation, low cost, fast response, high sensitivity and selectivity [4, 5]. Dopamine (DA) as one of the key neurotransmitters in the central nervous system, is associated with several neurological diseases such as Parkinson's disease and drug addiction [6]. Therefore, it is necessary to develop a suitable and effective electrochemical method to detect dopamine in physiological state [7-9].

Graphene or reduced graphene oxidation (RGO) is a 2D material with a single layer of an sp^2 carbon atom network densely packed in a honeycomb structure with extraordinary thermal, electronic and mechanical properties [10]. Owing to its unique structural and electronic properties, RGO is considered as the most promising support for loading metal nanoparticles [11, 12]. Pd has the potential of industrialization because it is an element that can replace Pt with the unique advantage of lower cost and toxicity [13]. Currently, Pd nanoparticles have been considered as one of the most effective catalysts for application in electrocatalysis for alcohol oxidation [13-15] and electrochemical sensor [16-18]. In addition, gold nanoparticles can perform superior catalysis properties while it was immobilized on the suitable support to be fixed somewhere [19]. As reported, Au is demonstrated to be more electronegative compared to Pd, thus optimizing the strength of the surface adsorption and improving the stability in Pd-based nanomaterials after the incorporation of Au [20]. The bimetallic system can obtain the synergistically enhanced catalytic effect of Pd and Au nanoparticles as well as the change of geometric morphologyy [20]. Additionally, when P was incorporated into the Pd-Au catalyst, the synergistic effect was received from these components owing to the change of electronic structure and long-range disorder and short-range structure [21]. The low-coordination sites and defects in this structures can effectively promote the electrocatalytical efficiency [22-24].

In this work, we designed poly(diallyldimethylammonium chloride)-functionalized RGO (PDDA/RGO) as a versatile platform for the growth of ternary Pd-Au-P nanoparticles via a gas-liquid interface approach [22]. The Pd-Au-P-PDDA/RGO composite as an electrochemical DA sensor showed superior electrocatalytic activity toward DA oxidation by using cyclic voltammetry (CV). A wide linear range, low limit of detection (LOD) and good selectivity were obtained. In addition, this electrochemical sensor was successfully employed to determine the amount of DA in human serum samples, demonstrating that the sensitive electrochemical sensor can be a promising candidate for daily applications in the DA detection.

2. EXPERIMENTAL

2.1 Reagents

GO was supplied by Nanjing XFNANO Tech Co. Dopamine hydrochloride(HCl-DA), Ascorbic acid (AA) and Uric acid (UA) were purchased from Alfa Aesar. $PdCl_2$ and $HAuCl_4$ were obtained from Aladdin. $NaBH_4$, NaOH, NH_4Cl, $MgSO_4$ and KNO_3 were purchased from Beijing Chemical Factory (Beijing, China). Polyvinylpyrrolidone (PVP) and Polydimethyl diallyl ammonium chloride (PDDA) were supplied by Kwangfu Fine Chemical Industry (Tianjin, China). All the chemicals were analytical grade and used as received without further purification. Water used in all experiments was purified using a Millipore Q system.

2.2 Synthesis process of Pd-Au-P-PDDA/ RGO composite

The synthesis process of PDDA/GO matrix was as follows: First, 176 mg PVP was dissolved in

44 mL GO solution (0.25 mg/mL) and ultrasonic disperse for 30 min. Then, the liquid suspension was dispersed in 10 mL water after centrifugation and being washed for three times. Subsequently, the 0.5 mL PDDA (20 wt.%) and 40 mL KCl (0.625 M) mixture was added into the above 10 mL aqueous solution and ultrasonic for 1.5 h. Ultimately, the resulting dispersion was centrifuged three times and the obtained PDDA/GO was dispersed into 20 mL water.

On the basis of PDDA/GO, 264 μL of 0.1012 M $HAuCl_4$ solution was added to the dispersion under uniform bubbling and stirring. After stirring for 30 min, 6.25 mL NaH_2PO_4•H_2O (0.8612 M) solution was added dropwise and the pH of the reaction system was adjusted to 8-9 with 0.1 M NaOH at the same time. Immediately, 1.50 mL $PdCl_2$ (0.0536 M) solution was quickly added. The reaction was continued with bubbling for 4 h at room temperature. After the reaction is completed, the 38.4 mg black solid powder of Pd-Au-P-PDDA/RGO was obtained by centrifugation and being washed with ethanol and water.

The synthesis of Pd-Au-PDDA/RGO was similar to that of Pd-Au-P-PDDA/RGO except for the process of adding $PdCl_2$ and adjusting pH. The 28.2 mg black solid particles were obtained from centrifugal filtration, washing and drying 3 times.

For comparison, Pd-Au-P/RGO was prepared according to the process of Pd-Au-P-PDDA/RGO However, the difference is the procedure of PDDA is deleted. Ultimately, the 42.6 mg black solid powder of Pd-Au-P/RGO was obtained after washing by centrifugation and being washed for three times.

2.3 Characterization

Transmission electron microscopy (TEM) was investigated by a Tecnai G2 F30 (FEI, USA). The fabrication of samples for TEM was performed by placing a drop of as-prepared solution on carbon-coated copper grids. The phase structures of the samples were measured from X-ray powder diffraction (XRD) analysis (Rigaku D/max-2400, Cu K-Alpha radiation, λ= 0.1541 nm). X-ray photoelectron spectroscopy (XPS) was acquired by a multifunctional spectrometer (Thermo Scientific) using Al Radiation.

2.4 Electrochemical measurements

All the electrochemical measurements were performed on a CHI 832B electrochemical workstation (Chenhua, Shanghai China). The conventional three electrode system was used with GCE as a working electrode (a diameter of 3 mm), saturated calomel electrode (SCE) as a reference electrode and Pt wire as a counter electrode. In particular, 1.0 mg Pd-Au-P-PDDA/RGO was dispersed in 1 mL ultrapure water (UPW) with 5 μL Nafion@117 solution (0.5wt%) to form a uniform suspension. 7 μL suspension was coated on GCE surface uniformly. The other materials modified on the GCE were prepared in the same manner as described.

3. RESULTS AND DISCUSSION

3.1 Characterization of Pd-Au-P-PDDA/RGO composite

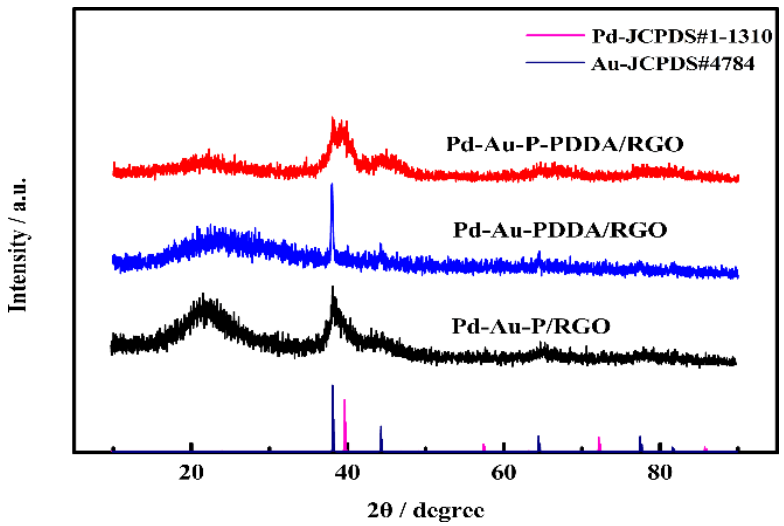

Figure 1. XRD patterns of Pd-Au-P/PDDA/RGO, Pd-Au-PDDA/RGO and Pd-Au-P/RGO.

The successful synthesis of Pd-Au-P nanoparticles on the PDDA/RGO was confirmed by XRD (Figure 1). PDDA was used as a functional material to prepare the stable cationic polyelectrolyte-functionalized graphene oxide and anchored Pd and Au alloy preventing them from growth and agglomeration during the reaction process[25].

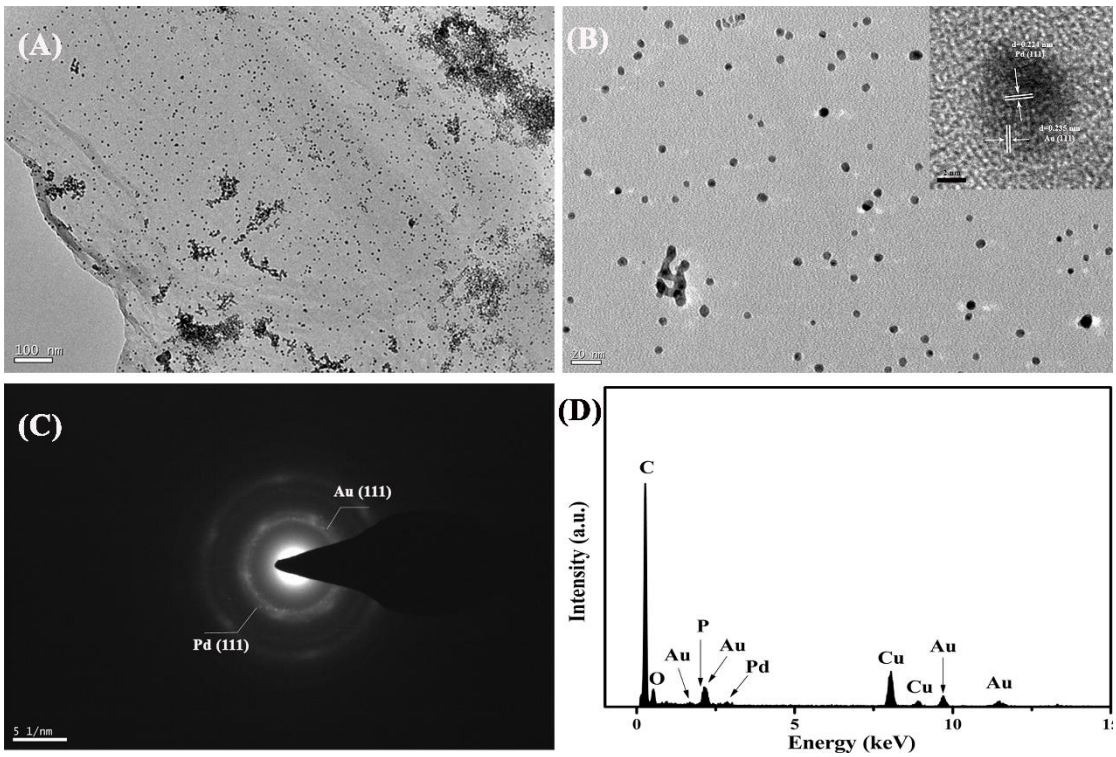

Figure 2. Characterization of Pd-Au-P/PDDA/RGO: TEM (A, B) and SAED (C) images, EDX spectrum (D). The inset of (B) shows the corresponding HRTEM image.

The enrichment immobilization of metallic nanoparticles was evidenced by XRD pattern in which the broad peaks located in 38-42° representing Pd-Au alloy in the Pd-Au-P-PDDA/RGO was broader and more abundant than Pd-Au-P/RGO. The XRD results show that diffraction peaks of Pd-Au-P/RGO shifted negatively compared with Pd-Au-PDDA/RGO, indicating an expansion of the Pd and Au lattice due to incorporation of P atoms [24].

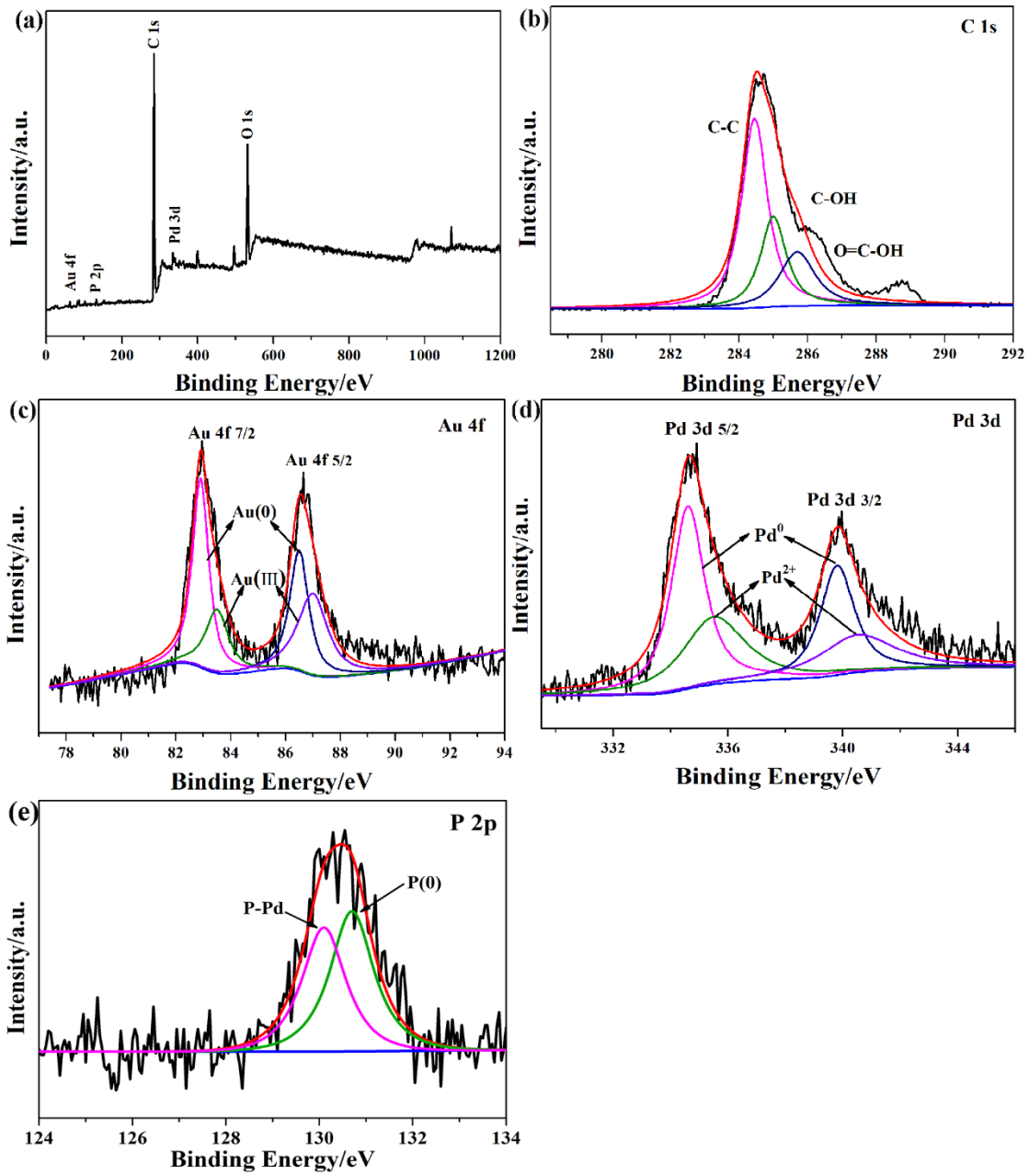

Figure 3. XPS characterization of Pd-Au-P/PDDA/RGO: (a) survey spectrum, (b) C 1s, (c) Au 4f, (d) Pd 3d, (e) P 2p.

In addition, the peak ~22° is the characteristic peak of graphene, which reflects the successful preparation of the Pd-Au-P-PDDA/RGO sample. The morphological characterization of Pd-Au-P-PDDA/RGO was performed by TEM. From the low-magnification TEM image (Figure 2A), it is clearly seen that highly dispersed metal nanoparticles are uniformly distributed on the wrinkled graphene sheets,

which can be attributed to the strong electrostatic interaction and coordination between the Pd-Au-P nanoparticles and the PDDA-modified graphene support [26]. Figure 2B further performs the average diameter of Pd-Au-P-PDDA/RGO is about 5 nm and the HRTEM image (the inset of Figure2B) demonstrates the lattice fringes with the spacing of 0.224 nm and 0.235 nm are assigned to Pd (111) [27] and Au (111) [28], respectively. The crystal lattices were also certificated by SAED pattern in Figure 2C, where the Pd (111) and Au (111) planes are clearly observed. The EDX spectrum shown in Figure 2D reveals the existence of Pd, Au and P in the Pd-Au-P-PDDA/RGO.

XPS measurement was further employed to analyze the chemical state of Pd-Au-P-PDDA/RGO. From the survey spectrum (Figure 3a), the elements like C 1s, Pd 3d, Au 4f and P 2p can be seen. Through high-resolution spectra and peak fitting, the peak of C 1s (Figure 3b) contains three characteristic peaks of C-C, C-OH and O=C-OH, indicating the presence of RGO [29]. In Au 4f XPS spectrum (Figure 3c), the binding energy (BE) peaks at 83.8 and 87.5 eV are attributed to the Au $4f_{7/2}$ and Au $4f_{5/2}$ spin-orbits (respectively), which are the characteristic peaks of Au^0 [30]. Except the Au^0, a second component corresponds to a cationic Au species (Au^{3+}) [30]. Figure 3d shows the high-resolution Pd 3d spectra, where the peaks of Pd^0 and Pd^{2+} can be clearly deconvoluted [31]. For P 2p peak, it can be fitted to two peaks: one is assigned to P (0), which can shorten the Pd-Au distance causing P doping [23]; the other belongs to the formation of Pd-P [31].

3.2 Electrocatalytic activity for DA oxidation

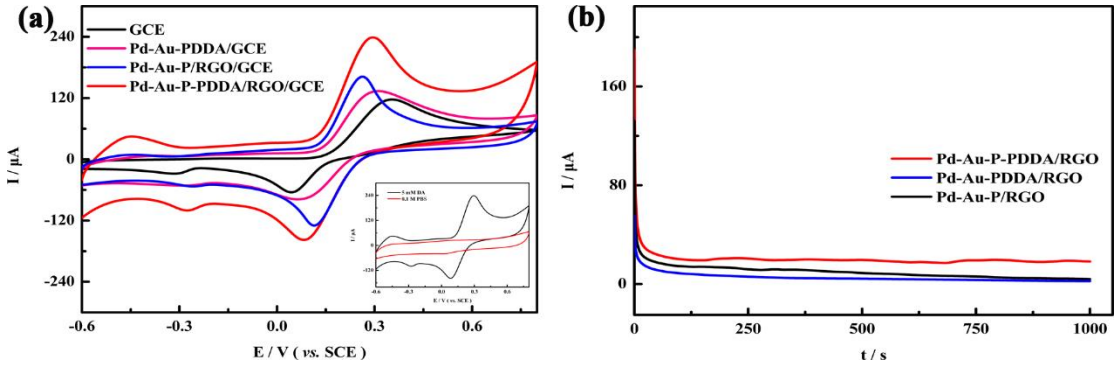

Figure 4. Electrochemical measurement of several materials of Pd-Au-P/PDDA/RGO, Pd-Au-P/RGO and Pd-Au/PDDA/RGO: (a) CVs of different materials modified on GCE in 5 mM dopamine; (b) I-t stability of corresponding material in 5 mM dopamine (pH=6.5). The inset of (a) show comparison chart of Pd-Au-P-PDDA/RGO modified GCE in 0.1 M PBS (red line) and 5 mM dopamine (black line). (scan rate :100 $mV \cdot s^{-1}$)

To investigate the electrochemical dopamine sensing performance, we performed the cyclic voltammetry (CV) measurements in 0.1 M PBS (pH 6.5) solution containing 5 mM DA over the materials. As shown in Figure 4a. the oxidation peak currents of the GCE modified with metallic catalysts are significantly greater than that of bare GCE, which indicates that the Pd-Au-based materials have efficient response to dopamine oxidation. And the electrooxidation peak current is the highest among these modified electrodes prepared from Pd-Au-P-PDDA/RGO, Pd-Au-P/RGO and Pd-Au-PDDA/RGO. Meanwhile, Pd-Au-P-PDDA/RGO has the smallest oxidation peak potential and the best

catalytic stability from the *i-t* curves (Figure4b), which further indicates that the addition of phosphorus can increase the activity and stability of the Pd-Au system. It is possibly attributed to the synergistic effect among Pd, Au and P atoms and the enhanced stability of the material from the electrostatic interaction between the functionalized RGO and metal nanopaticles[22-24]. Importantly, the enhancement from the phosphorus element in the ternary system is pronounced due to the incorporation of P into the lattice interstices[23,24].

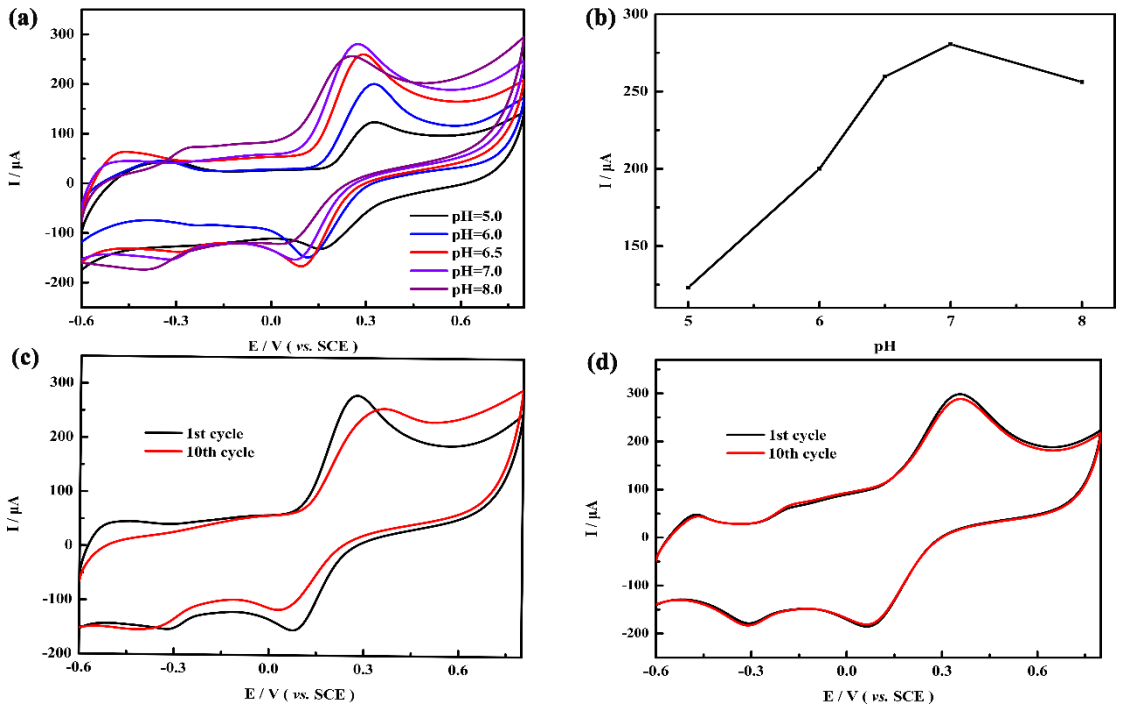

Figure 5. The response of solution pH based on Pd-Au-P-PDDA/RGO modified on GCE in the PBS solution: (a) CVs of different pH (5.0~8.0); (b) Plot of I versus pH. CV curves from the first to the 10th lap in 0.1M PBS with 5 mM DA at pH=7.0 (c) and pH= 6.5 (d), the scan rate: 50 mV/s.

Due to the polymerization properties of DA in alkaline conditions [7], it is important to select pH for sensing DA. Figure 5a shows the CV curves of DA oxidation corresponding to different pH values, and the distribution diagram of current vs pH is shown in Figure 5b. It is found that the maximum peak current appears at pH 7.0. However, the stability at pH 7.0 is not ideal after scanning ten times, where the deceased oxidation current and positive shift of oxidation potential are seen in Figure 5c. In contrast, for pH 6.5, the comparison between the first scanning cycle and the tenth scanning cycle shows basic coincidence of the CV curves (Figure 5d). So, we selected pH 6.5 for the following experiments.

3.3 Kinetic study

The kinetic behavior of DA oxidation on Pd-Au-P-PDDA/RGO modified GCE was investigated by varying the scan rate (ν) (Figure 6a). As be seen, the oxidation peak potential (E_{pa}) shifts positively

as the scanning rate increases; simultaneously, both oxidation and reduction current increase with the increase of scan rate.

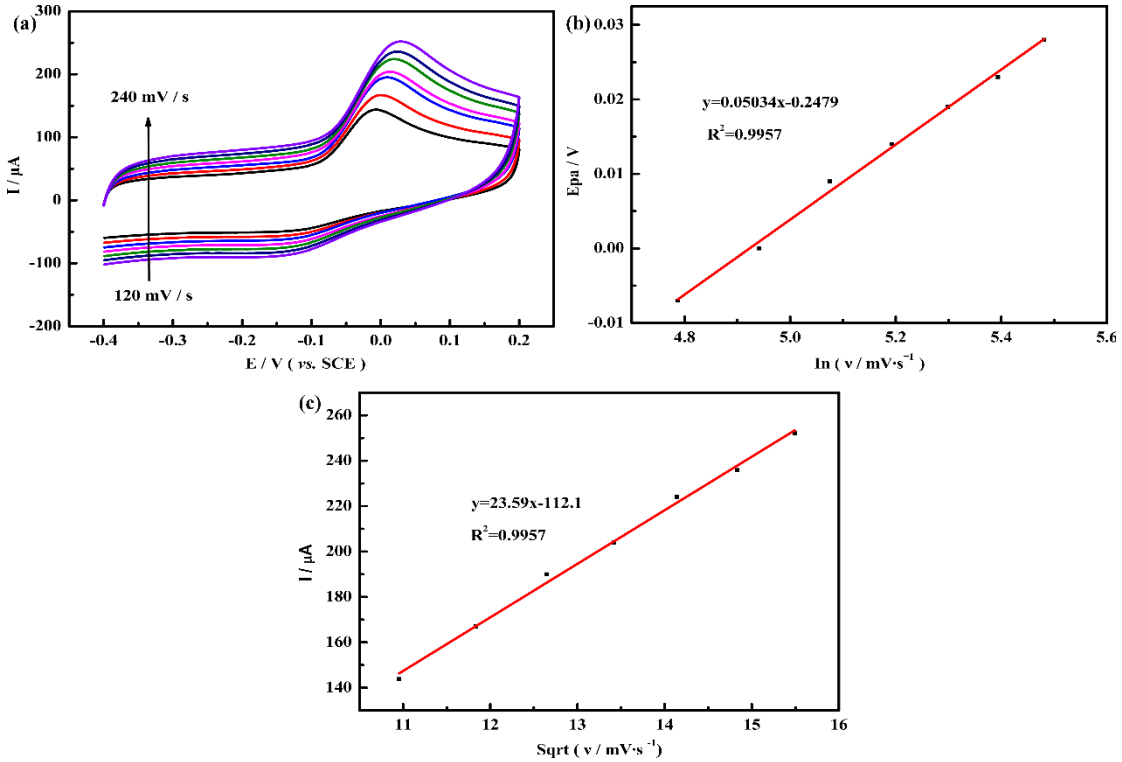

Figure 6. (a) CVs of dopamine oxidation over Pd-Au-P/PDDA/RGO under different scan rate 120-240 mV/s; (b) the linear calibration plot of E_{pa} *vs* ln(v); (c) the linear relationship between I_{pa} and $v^{1/2}$.

The linear relationship between the E_{pa} and the natural logarithm of the scanning speed (ln$v$) was shown in Figure 6b. The linear regression equation is E_{pa} = 0.1450 + 0.03079 ln$v$ (R^2 = 0.9990). For an irreversible electrochemical process, E_{pa} follows Laviron's equation [32]:

$$Epa = E_0 + (RT/(1-\alpha)nF)\ln(RTk^0/(1-\alpha)nF) + (RT/(1-\alpha)nF)\ln v \quad (1)$$

where n is the number of transfer electrons, α is the electron transfer coefficient, v is the sweep speed, E^θ is the standard redox potential and k^θ is the standard isomerization rate constant of the reaction. According to the reported literature [33], the slope of the above formula can be used to calculate the obtained electron transfer coefficient α = 0.723, while the number of transfer electrons in the oxidation of dopamine is 2. In addition, the relationship between the oxidation peak current (I_{pa}) and the square root of the sweep speed Sqrt(v) in Figure 6c satisfies the linear equation of I_{pa} = 15.69 + 25.61 $v^{1/2}$ (R^2 = 0.9994), indicating that dopamine catalyzed by Pd-Au-P-PDDA/RGO is a typical diffusion control process [32, 33].

3.4 Amperometric determination of DA

Differential pulse method (DPV) was applied for the amperometric determination of DA based

on Pd-Au-P-PDDA/RGO modified GCE in 0.1 M PBS (pH = 6.5). It can be seen that the oxidation current increases with the DA concentration (Figure 7a). A linear response of the Logarithm of I_{pa} against the DA concentration is illustrated in Figure 7b.

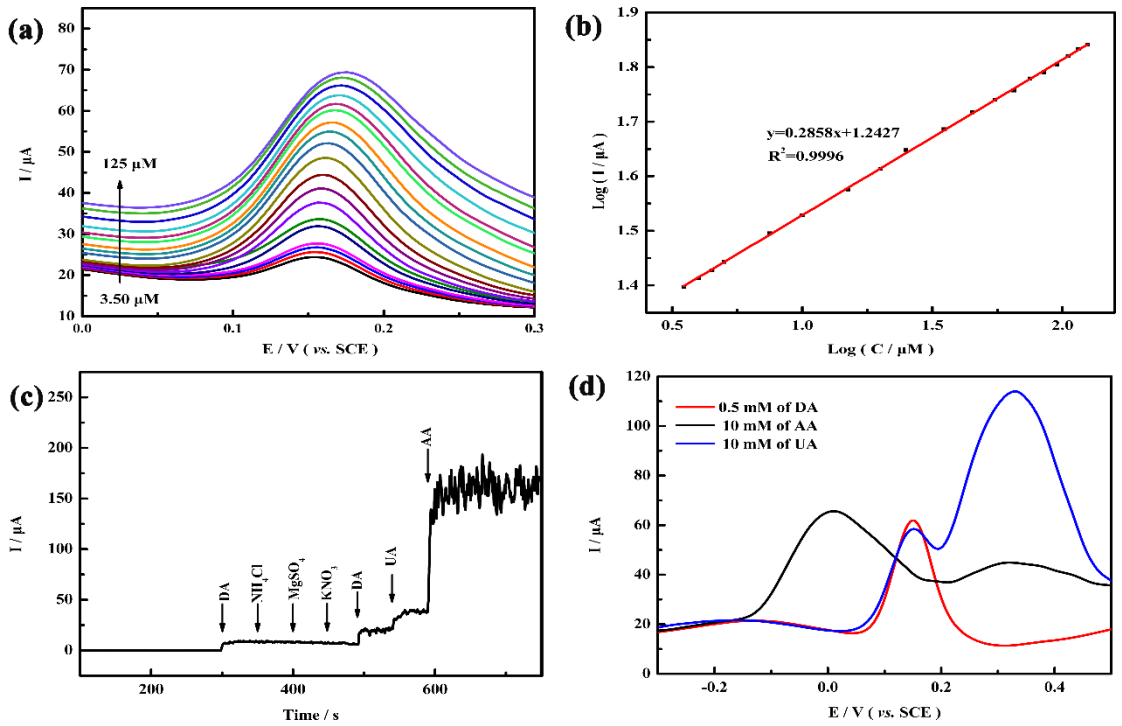

Figure 7. Electrochemical determination of dopamine based on Pd-Au-P/PDDA/RGO modified on GCE: (a) DPV curves; (b) Linear calibration plot of Log(I_{pa}) vs Log(C_{DA}); (c) I-t curve originating from the anti-interference of various compounds including NH_4Cl, $MgSO_4$, KNO_3, AA, UA and DA; (d) DPV curves of 0.5 mM DA, 10 mM AA and 10 mM UA.

Table 1. Comparison of the electrochemical response for DA detection based on Pd-Au-P-PDDA/RGO and other electrochemical materials.

Electrode material	Detection method	pH	Detection Potential(V)	Linear range(μM)	LOD (μM)	Ref.
PILs/PPy/GO[a]	DPV	4.0	0.4	4-18	0.073	[31]
PEDOT-LSG[b]	DPV	7.4	0.277	1-150	0.33	[32]
3DG-CNTN[c]	CV	6.0	0.111	0.7-100	0.070	[33]
ERGO-PLL[d]	DPV	7.4	0.228	2.0-60	0.10	[34]
HNP-PtTi[e]	DPV	7.0	0.46	4-500	3.20	[35]
PtAg/RGO[f]	DPV	6.0	0.235	0.4-96.0	0.048	[36]
Pd-Au-P/PDDA/RGO	DPV	6.5	0.164	3.5-125	0.70	This work

[a] poly (ironic liquids) functionalized polypyrrole/graphene oxide nanosheets (PILs/PPy/GO)
[b] poly (3,4-ethylenedioxythiophene) modified laser scribed graphene (PEDOT-LSG)
[c] hierarchical nanoporous PtTi alloy (HNP-PtTi)
[d] porous bimetallic alloyed PdAg nanoflowers supported on reduced graphene oxide (PtAg/RGO)
[e] 3D porous graphene-carbon nanotube (3DG-CNTN)
[f] electrodeposited reduced graphene oxide incorporating polymerization of L-Lysine (ERGO-PLL)

The linear range is 3.5 - 125 μM with high sensitivity of 0.2858 μA/μM and the LOD is only 0.7 μM. Compared to non-metallic materials such as PILs/PPy/GO [34], PEDOT-LSG[35], 3DG-CNTN[36], ERGO-PLL [37] and noble metal-based catalysts like HNP-PtTi[38] and PtAg/RGO[39] materials, the Pd-Au-P-PDDA/RGO sensor has obvious advantages of lower LOD and wider linear range, as seen in Table 1. So, this electrochemical sensor is suitable for bioelectrochemical detection of DA.

Another important factor for electrochemical DA sensor is the ability of resisting interference. Here, the anti-interference test is shown in Figure 7c, where the concentrations of interfering species reach up to 20 folds of 0.5 mM DA. It can be seen that the sensor has nearly no response to K^+, Na^+, NH_4^+, Cl^-, NO_3^- while there is a very obvious electrochemical response to the addition of DA. Although the addition of ascorbic acid (AA) and uric acid (UA) with a high concentration can bring a slight response, we can easily control the oxidation potential to distinguish their detection against the detection of DA. From Figure 7d, the oxidation potentials toward the oxidation of DA, AA and UA are different. It can be inferred that this sensor has the possibility of simultaneous determination of DA, AA, UA, considering their distinguished peaks.

3.5 Applications in real sample analysis

In order to evaluate the reliability of the Pd-Au-P-PDDA/RGO in practical applications, we detected the DA content in human blood samples based on this electrochemical sensor. Prior to the measurement, the blood samples were pre-treated as follows: the blood samples were centrifuged at 11000 rpm for 5 min to remove the protein, and then diluted 50-fold with 0.1 M PBS solution. Due to the low content of DA in the samples, the standard recovery method was used to assess the accuracy of the DA content in human blood samples. Three parallel measurements were performed. The recoveries of the measured samples were 98.4-102.6% when five different DA concentrations were added into the blood sample, as shown in Table 2. The relative standard deviation (RSD) values were limited within 3.2%. The satisfactory results show that the measurement method has good accuracy for the detection of real samples.

Table 2. Determination of DA in human serum samples (n=3).

Sample	Added(μM)	Found(μM)	Recovery(%)	RSD(%)
1	15.00	15.40	102.6	2.43
2	30.00	29.52	98.4	3.08
3	45.00	46.06	102.4	1.80
4	60.00	59.88	99.8	3.14
5	75.00	75.23	100.3	2.62

4. CONCLUSIONS

In this work, we synthesized ternary Pd-Au-P-PDDA/RGO composites via a gas-liquid interface approach, successfully proving that phosphorus was incorporated into a bimetallic Pd-Au system. The synergistic enhancement of the material improved the activity and stability toward DA oxidation and simultaneously enhanced the detection sensitivity and selectivity. Electrochemical measurements exhibited high amperometric response, low LOD, wide linear range and good anti-interference. By using standard addition method to detect the DA content in human serum samples, the recoveries were in the range of 98.4-102.6% and the RSD values only limited within 3.2%. It is believed that the Pd-Au-P-PDDA/RGO material has promising advantages in the detection of DA and application prospects in practical measurements.

ACKNOWLEDGEMENT
This work is supported by the Fundamental Research Fund for the Central Universities (lzujbky-2017-144).

References

1. S. Yang, X. Sun, Z. Wang, X. Wang, G. Guo, Q. Pu, *Sens. Actuat. B*, 253 (2017) 752.
2. N. Li, J. Guo, B. Liu, Y. Yu, H. Cui, L. Mao, Y. Lin, *Anal. Chim. Acta* , 645 (2009) 48.
3. X. Fang, H. Ren, H. Zhao, Z. Li, *Microchim. Acta* , 184 (2017) 415.
4. Q. Yuan , Y. Liu, C. Ye, H. Sun, D. Dai, Q. Wei, G. Lai, T. Wu, A. Yu, L. Fu , K. W. A. Chee, C. Lin, *Biosen. Bioelectron.*, 111 (2018) 117.
5. H. Jin, C. Zhao, R. Gui, X. Gao, Z. Wang, *Anal. Chim. Acta*, 1025 (2018) 154.
6. G. D. Stuber, M. Klanker, B. Ridder, M. S. Bowers, R. N. Joosten, M. G. Feenstra, A. Bonci, *Science*, 321 (2008) 1690.
7. X. Xia, X. Shen, Y. Du, W. Ye, C. Wang, *Sens. Actuat. B*, 237 (2016) 685.
8. L. Ma, Zhang, Q. Zhang, C. Wu, Y. Zhang, L. Zeng, *Anal. Chim. Acta*, 1055 (2019) 17.
9. L. Wang, R. Yang, J. Li, L. Qu, P. D. Harrington, *Talanta*, 196 (2019) 309.
10. D. Li, M. B. Muller, S. Gilje, R. B. Kaner, G. G. Wallace, *Nat. Nanotechnol*, 3 (2008) 101.
11. W. Ye, J. Yu, Y. Zhou, D. Gao, D. Wang, C. Wang, D. Xue, *Appl. Catal. B-Environ.*, 181 (2016) 371.
12. C. Zou, J. Zhong, S. Li, H. Wang, J. Wang, B. Yan, Y. Du, *J. Electroanal. Chem.,* 805 (2017) 110.
13. D. Rajesh, P. I. Neel, A. Pandurangan, C. Mahendiran, *Appl. Surf. Sci.,* 442 (2018) 787.
14. M. Melchionna, M. V. Bracamonte, A. Giuliani, L. Nasi, T. Montini, C. Tavagnacco, M. Bonchio, P. Fornasiero, M. Prato, Pd@TiO_2/carbon nanohorn electrocatalysts: reversible CO_2 hydrogenation to formic acid. *Energy Environ. Sci.,* 11 (2018) 1571.
15. I. M. A. Mohamed, A. S. Yasin, N. A. M. Barakat, S. A. Song, H. E. Lee, S. S. Kim, *Appl. Surf. Sci.,* 435 (2018) 122.
16. Z. Gao, Y. Li, X. Zhang, J. Feng, L. Kong, P. Wang, Z. Chen, Y. Dong, Q. Wei, *Biosens. Bioelectron.,* 102 (2018) 189.
17. Z. Zhao, Z. Xia, C. Liu, H. Huang, W. Ye, *Electrochim. Acta,* 256 (2017) 146.
18. Z. Zheng, Y. Du, Q. Feng, Z. Wang, C. Wang, *J. Mol. Catal. A,* 353-354 (2012) 80.
19. S. H. Kim, *Current Appl. Phys.,* 18 (2018) 810.
20. C. Ye, M. Wang, X. Zhong, S. Chen, Y. Chai, R. Yuan, *Biosens. Bioelectron.,* 79 (2016) 34.

21. T. Li, Y. Wang, Y. Tang, L. Xu, L. Si, G. Fu, D. Sun, Y. Tang, *Catal. Sci. Technol.,* 7 (2017) 3355.
22. Y. Ma, H. Wang, W. Lv, S. Ji, B. G. Pollet, S. Lia, R. Wang, *RSC Adv.* 5 (2015) 68655.
23. H. Huang, H. Wang, W. Hu, W. Lv, W. Ye, *Electrochem. Commun.,* 82 (2017) 107.
24. L. Chen, L. Lu, H. Zhu, Y. Chen, Y. Huang, Y. Li, L. Wang, *Nat. Commun.,* 8 (2017) 14136.
25. K. Liu, J. Zhang, G. Yang, C. Wang, J. Zhu, *Electrochem. Commun.,* 12 (2010) 402.
26. Q. Yuan , Y. Liu, C. Ye, H. Sun, D. Dai, Q. Wei, G. Lai, T. Wu, A. Yu, L. Fu , K. W. A. Chee, C. Lin, *Biosen. Bioelectron.,* 111 (2018) 117.
27. H. Jin, C. Zhao, R. Gui, X. Gao, Z. Wang, *Anal. Chim. Acta,* 1025 (2018) 154.
28. G. D. Stuber, M. Klanker, B. Ridder, M. S. Bowers, R. N. Joosten, M. G. Feenstra, A. Bonci, *Science,* 321 (2008) 1690.
29. Y. Ma, C. Si, X. Yang, J. Li, Z. Wang, X. Shi, W. Ye, P. Zhou, W. M. Budzianowski, *J. Colloid Interf. Sci.*, 552 (2019) 72.
30. H. Huang, T. Li, Y. Sun, L. Yu, C. Wang, R. Shen, W. Ye, D. Wang, Y. Li, *Microchim. Acta*, 186 (2019) 46.
31. Z. Zhao, X. Ma, X. Wang, Y. Ma, C. Liu, H. Huang, Zhang, Y.; Du, Ye, W. *Appl. Surf. Sci.* 457 (2018) 1009-1017.
32. L. Wang, R. Yang, J. Li, L. Qu, P. D. Harrington, *Talanta,* 196 (2019) 309.
33. W. Ye, Y. Chen, Y. Zhou, J. Fu, W. Wu, D. Gao, F. Zhou, C. Wang, D. Xue, *Electrochim. Acta,* 142 (2014) 18.
34. H. Mao, J. Liang, H. Zhang, Q. Pei, D. Liu, S. Wu, Y. Zhang, X. Song, *Biosens. Bioelectron.*, 70 (2015) 289.
35. G. Xu, Z. A. Jarjes, V. Desprez, P. A. Kilmartin, J. Travas-Sejdic, *Biosens. Bioelectron.*, 107 (2018) 184.
36. E. Asadian, S. Shahrokhian, A. I. Zad, F. Ghorbani-Bidkorbeh, *Sens. Actuat. B-Chem.*, 239 (2017) 617.
37. D. Zhang, L. Li, W. Ma, X. Chen, Y. Zhang, *Mater. Sci. Eng. C*, 70 (2017) 241.
38. D. Zhang, G. Yu, K. Tian, C. Xu, *Biosens. Bioelectron.*, 82 (2016) 119.
39. L. Chen, J. Zheng, A. Wang, L. Wu, J. Chen, J. Feng, *Analyst*, 140 (2015) 3183.